Superconducting Grid-Bus Surface Code Architecture for Hole-Spin Qubits

Simon E. Nigg,[1,*] Andreas Fuhrer,[2] and Daniel Loss[1]
[1]Department of Physics, University of Basel, Klingelbergstrasse 82, 4056 Basel, Switzerland
[2]IBM Research—Zurich Säumerstrasse 4, 8803 Rüschlikon, Switzerland
(Received 10 January 2017; published 3 April 2017)

We present a scalable hybrid architecture for the 2D surface code combining superconducting resonators and hole-spin qubits in nanowires with tunable direct Rashba spin-orbit coupling. The backbone of this architecture is a square lattice of capacitively coupled coplanar waveguide resonators each of which hosts a nanowire hole-spin qubit. Both the frequency of the qubits and their coupling to the microwave field are tunable by a static electric field applied via the resonator center pin. In the dispersive regime, an entangling two-qubit gate can be realized via a third order process, whereby a virtual photon in one resonator is created by a first qubit, coherently transferred to a neighboring resonator, and absorbed by a second qubit in that resonator. Numerical simulations with state-of-the-art coherence times yield gate fidelities approaching the 99% fault tolerance threshold.

DOI: 10.1103/PhysRevLett.118.147701

Scalability is central to the ongoing efforts towards fault tolerant quantum computation [1–9]. Owing to its high error rate threshold and its benign requirement of only local qubit interactions, the surface code [10] is a promising candidate to achieve fault tolerance. Superconducting circuits, with their long coherence times and high-level of controllability, have emerged as an ideal platform for a physical implementation of the surface code [11–17]. At the heart of this approach lies the coherent light-matter interaction between the electric dipole moment of a superconducting condensate and quantized microwave fields [18]. This interaction, however, is a double-edged sword. On the upside, it enables the readout and control of superconducting qubits and of their interaction with each other via the quantum bus [19,20]. On the downside, the presence of an electric dipole moment means that unmonitored degrees of freedom, such as thermal and quantum fluctuations of the field, couple to the qubits and limit their coherence [21]. Moreover, in a multiqubit system, the accumulation of errors due to off-resonant couplings represents a serious problem for scalability [15–17,22]. The ability to tune the light-matter coupling on and off on demand is thus highly desirable. Superconducting qubits with tunable qubit-resonator coupling have been realized [23–26], but their robustness is limited since they rely on quantum coherent interference at a symmetry point.

The recent discovery [27] of an electrically induced spin-orbit interaction of Rashba type in the low energy hole states of Ge/Si (core/shell) nanowires provides an attractive alternative to realize a tunable coupling qubit. In this case the qubit is encoded in two orthogonal dressed spin states of a hole confined in a nanowire quantum dot. Hole spins are particularly attractive since their p-wave orbitals have minimal overlap with the nuclei resulting in long coherence times [28–31] and have recently been demonstrated to be compatible with industrial CMOS technology [32]. Crucially the strong direct Rashba spin-orbit interaction (DRSOI) is controlled by an *external* electric field applied perpendicular to the wire [27,29]. This enables the electrostatic control of the coupling between the spin degree of freedom and the electromagnetic field along the wire.

In this Letter, we propose a scalable surface code architecture obtained by combining nanowire hole-spin qubits with a novel coplanar waveguide resonator grid structure. The latter can be viewed as a generalization of the celebrated 1D quantum bus architecture [19,20] to two dimensions. Furthermore, owing to the small size of the hole-spin qubits, a few tens of nanometers in length, they can be entirely embedded within the microwave resonators allowing for more compact resonator geometries with enhanced vacuum field strengths. The electrostatic fields required to tune the microwave-qubit coupling, are provided *in situ* by voltage biasing the resonator center conductor thus reducing the number of required leads.

The system we consider is depicted schematically in Fig. 1. It consists of a square lattice of coplanar microwave resonators, with a hole-spin qubit placed at the field antinode of each resonator. Here we consider full-wave resonators where the resonator length equals the wavelength λ and the qubits are placed at the central antinode. Each resonator is capacitively coupled to four neighboring resonators forming a horizontal "H" shape as shown in Fig. 1(g). The nanowires, each containing a single hole-spin qubit, are situated inside the trenches between the center conductor and the ground plane defining the resonator, as depcited in insets (b) and (e) of Fig. 1. The qubit is thus fully embedded within the resonator. The electromagnetic fields are only weakly screened inside the semiconductor of the nanowire enabling a strong coupling between the qubit and the ac field component along the wire [29].

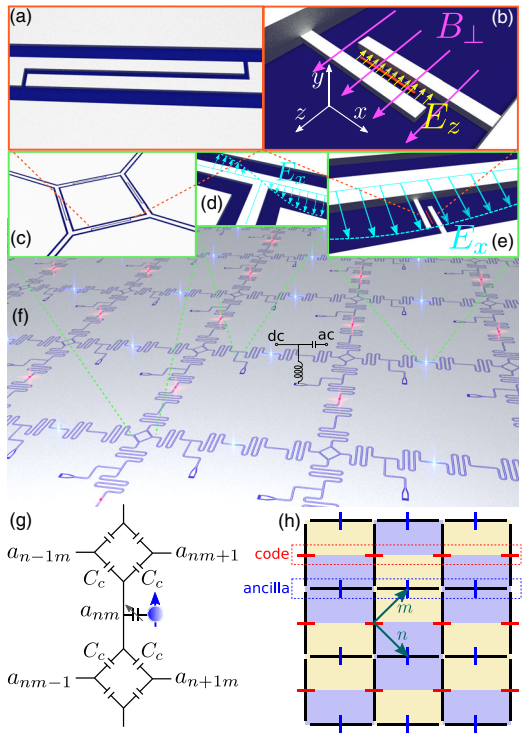

FIG. 1. Grid-bus surface code architecture. (a) and (c) Four-way capacitor design minimizing undesired cross-couplings. (b) and (e) A nanowire hole-spin qubit inside a capacitor in the trench of the resonator. The electric field perpendicular to the wire E_z is controlled by voltage biasing the center conductor via the bias-tee shown in (f). (d) Resonator drive port placed at a node of the ac field E_x. (f) Resonator grid layout. The light gray areas represent the superconductor thin film on top of the dielectric substrate (dark blue). The red and blue dots at the center of each resonator indicate the positions of the hole-spin qubits. (g) Each resonator couples to four neighboring resonators. (h) Resonator (black lines) and qubits (red and blue bars) arranged in a square lattice. The red bars denote code qubits while the blue bars denote ancilla qubits. The colored rectangles represent the two types of plaquettes of the surface code (e.g., $XXXX$ or $ZZZZ$). The basis vectors on the lattice are indicated by dark green arrows labeled n and m.

To characterize this system, we start by considering an isolated site of the lattice composed of one resonator and one hole-spin qubit. The nanowire containing the qubit is oriented along the x axis and a magnetic field is applied along z. We describe the hole harmonically confined along the wire by the 1D effective Hamiltonian [33]

$$\boldsymbol{H}_h = \frac{\boldsymbol{p}^2}{2m} + \frac{1}{2}m\omega_h^2\boldsymbol{x}^2 + \alpha_{\mathrm{DR}}\boldsymbol{\sigma}^y\boldsymbol{p} + \frac{g\mu_B B_\perp}{2}\boldsymbol{\sigma}^z. \quad (1)$$

Here, α_{DR} is the strength of the DRSOI and $B_\perp$ denotes the magnetic field strength perpendicular to the axis of the wire. The hole furthermore couples to the electromagnetic field of the resonator and this is described in dipole approximation via the Hamiltonian $\boldsymbol{H}_r = eE_{\mathrm{rms}}\boldsymbol{x}(\boldsymbol{a}+\boldsymbol{a}^\dagger)+\hbar\omega_r\boldsymbol{a}^\dagger\boldsymbol{a}$. Here $E_{\mathrm{rms}} = 1/W\sqrt{\hbar\omega_r/cl}$ is the x component of the antinode vacuum root mean square field of the coplanar waveguide (CPW) resonator with resonance frequency ω_r, trench width W, length l and capacitance per unit length c. The full Hamiltonian is $\boldsymbol{H} = \boldsymbol{H}_h + \boldsymbol{H}_r$. The effect of the spin-orbit coupling is seen most clearly upon performing the unitary transformation $\boldsymbol{U} = \exp[i(\boldsymbol{x}/\ell_{\mathrm{SO}})\boldsymbol{\sigma}^y]$, where the spin-orbit length $\ell_{\mathrm{SO}} = \hbar/(m\alpha_{\mathrm{DR}})$ characterizes the length over which the spin flips due to spin-orbit coupling in the absence of a magnetic field. This generalizes the semiclassical approach of Refs. [34,35] to the quantum regime. In the limit where $\ell_{\mathrm{SO}} \gg x_{\mathrm{ZPF}} = \sqrt{\hbar/(2m\omega_h)}$, the mixing of orbital and spin degrees of freedom is weak and the transformed Hamiltonian reads [36]

$$\boldsymbol{H} \simeq \boldsymbol{H}_r + \frac{\boldsymbol{p}^2}{2m} + \frac{1}{2}m\omega_h^2\boldsymbol{x}^2 + \frac{\hbar\omega_Z}{2}\left(\boldsymbol{\sigma}^z - \frac{2\boldsymbol{x}}{\ell_{\mathrm{SO}}}\boldsymbol{\sigma}^x\right). \quad (2)$$

Here we have suppressed a c-number term and defined the Zeeman frequency $\omega_Z = g\mu_B B_\perp/\hbar$.

We are interested in the regime where $\omega_h \gg \omega_r, \omega_Z$ such that the hole remains in its ground state and we can adiabatically eliminate the center of mass motion of the hole [36]. The dynamics of the hole spin coupled to the resonator is then captured by an effective Jaynes-Cummings model

$$\frac{\boldsymbol{H}_{\mathrm{JC}}}{\hbar} = \omega_r\boldsymbol{a}^\dagger\boldsymbol{a} + \frac{\omega_Z'}{2}\boldsymbol{\sigma}^z + \nu(\boldsymbol{a}\boldsymbol{\sigma}^+ + \boldsymbol{a}^\dagger\boldsymbol{\sigma}^-), \quad (3)$$

where the transition frequency of the qubit is determined by the renormalized Zeeman splitting

$$\omega_Z' = \omega_Z\left[1 - \frac{\omega_Z}{\omega_h - \omega_Z}\left(\frac{x_{\mathrm{ZPF}}}{\ell_{\mathrm{SO}}}\right)^2\right], \quad (4)$$

and the spin-field coupling strength is given by

$$\hbar\nu = \frac{\beta\omega_Z}{\omega_h - \omega_r}\left(\frac{x_{\mathrm{ZPF}}}{\ell_{\mathrm{SO}}}\right). \quad (5)$$

Here, $\beta = eE_{\mathrm{rms}}x_{\mathrm{ZPF}}$ is the dipole coupling strength between the hole in the motional ground state and the vacuum field of the resonator. Importantly, ℓ_{SO} depends, via the spin-orbit coupling strength α_{DR}, on the electric field component E_z perpendicular to the wire. In the weak field limit $\alpha_{\mathrm{DR}} \propto E_z$ and the coupling ν increases linearly with E_z while ω_Z' decreases quadratically. Thus the "off" state, $E_z = 0$, corresponds to a sweet spot for the qubit where it is protected against fluctuations of the electric field to linear order. A nonperturbative treatment, of which the above expressions (4) and (5) are the leading order terms, can be found in Ref. [29]. For Ge/Si nanowires, the Zeeman splitting in Eq. (4) reaches the GHz frequency regime for magnetic field strengths around one hundred milli Tesla. We emphasize that our architecture is compatible with a magnetic field parallel to the plane of the superconducting resonator, mitigating adverse effects on the resonator quality factor [38]. Furthermore, the required electrostatic control field can be generated by applying a voltage bias between the center conductor and the ground plate of the resonator at a field node as depicted in inset (d) of Fig. 1. By using a bias tee, the same

port can be used to drive the resonator for the purpose of single-qubit operations as explained further below.

Scaling up, we next consider an $N \times M$ lattice of such resonators, where each resonator is coupled capacitively to four neighboring resonators as illustrated in Fig. 1(g). Because of the strong suppression of the g factor along the axis of the wires [39,40], we consider for each wire only the perpendicular component of the applied magnetic field justifying the applicability of Eq. (3) also in this case [36]. In the rotating wave approximation, the dynamics on the lattice can be modeled by the Jaynes-Cummings-Hubbard Hamiltonian [41]

$$\frac{\boldsymbol{H}}{\hbar} = \sum_{n=1}^{N}\sum_{m=1}^{M}\left(\frac{\omega_Z}{2}\boldsymbol{\sigma}_{nm}^{z} + \omega_r \boldsymbol{a}_{nm}^{\dagger}\boldsymbol{a}_{nm} + \nu_{nm}(\boldsymbol{a}_{nm}\boldsymbol{\sigma}_{nm}^{+} + \text{H.c.})\right) + J\sum_{n,m}(\boldsymbol{a}_{nm}^{\dagger}\boldsymbol{a}_{nm+1} + \boldsymbol{a}_{nm}^{\dagger}\boldsymbol{a}_{nm-1} + \boldsymbol{a}_{nm}^{\dagger}\boldsymbol{a}_{n+1m} + \boldsymbol{a}_{nm}^{\dagger}\boldsymbol{a}_{n-1m}). \tag{6}$$

The interresonator coupling strength is given by $J = 2\omega_r(C_c/C + 4C_c)$, in terms of the mode frequency ω_r, the coupling capacitance C_c, and the effective self-capacitance of the resonator mode $C = cl$. The tunable spin-resonator coupling of lattice site (n, m) is denoted with ν_{nm}.

A scalable implementation of the surface code requires (i) Two-qubit gates between nearest neighbors on a lattice. (ii) Arbitrary single-qubit rotations. (iii) Individual qubit readout in the computational basis. (iv) Parallelizability. Conditions (i) and (ii) together allow one to encode the error syndrome onto ancilla qubits and (iii) allows one to read out the error syndrome. Condition (iv) means that the gates must be performed in parallel so that the time for a single syndrome measurement cycle does not increase with the lattice size. In theory all stabilizer operator measurements could be done simultaneously, since per definition the stabilizer operators commute with each other. However, in practice when the measurements of multi-qubit stabilizer operators are decomposed into sequences of single and two-qubit gates between pairs of qubits, a certain degree of sequentiality is unavoidable. In the following we show how our architecture meets the requirements (i) to (iv).

Single-qubit gates.—To address a particular qubit, the center conductor of the corresponding resonator is voltage biased, generating an electric field $E_z = E_z^*$ perpendicular to the wire [see Fig. 1(b)]. This effectively turns on the DRSOI and couples the qubit to the ac field. Single-qubit rotations around any axis in the $x - y$ plane of the Bloch-sphere can then be performed in a standard way [18], by driving the resonator mode at the Lamb and Stark shifted qubit resonance frequency with a coherent microwave drive of appropriate phase [see Fig. 3(a) and [36]]. By concatenating rotations around different axes, arbitrary rotations on the Bloch sphere can be generated. Interestingly, the electric tunability of the Zeeman splitting provides a shortcut for single-qubit phase gates: To acquire a phase θ one simply has to bias the center conductor for a duration $T = \theta/\Delta\omega_Z$ with $\Delta\omega_Z = \omega_Z(E_z = 0) - \omega_Z(E_z = E_z^*)$. Because each resonator is coupled only to its four orthogonal neighboring resonators, single-qubit gates can be performed in parallel on all code qubits and separately on all ancilla qubits by alternatingly coupling one set of qubits to the grid bus while the other remains uncoupled.

Nearest neighbor two-qubit gates.—A high fidelity two-qubit gate can be realized by a generalization of the resonator-bus mediated qubit-qubit flip-flop interaction [18,19,29]. Since each qubit is directly coupled only to one resonator, a virtual photon emitted by the first qubit needs to hop from one resonator to a neighboring resonator before being absorbed by the second qubit [see Fig. 3(b)]. A perturbative analysis [36] gives an effective coupling between qubits at sites (n, m) and (n', m') of the form

$$\frac{\boldsymbol{H}_{XY}}{\hbar} = \sum_{nm,n'm'} K_{nm,n'm'}\boldsymbol{\sigma}_{nm}^{+}\boldsymbol{\sigma}_{n'm'}^{-} + \text{H.c.}, \tag{7}$$

where, in the weak coupling regime $J \ll |\omega_Z - \omega_r|$, the coupling strength is given by [36]

$$K_{nm,n'm'} = \frac{(\Delta m + \Delta n)!}{\Delta n!\Delta m!}\frac{\nu_{nm}\nu_{n'm'}}{\Delta}\left(\frac{J}{\Delta}\right)^{\Delta m+\Delta n}, \tag{8}$$

with $\Delta n = |n - n'|$, $\Delta m = |m - m'|$ and $\Delta = \omega_r - \omega_Z$. The coupling strength decays exponentially with distance on the lattice and the nearest neighbor coupling strength (i.e., for $n' = n$ and $m' = m \pm 1$ or $n' = n \pm 1$ and $m' = m$), is [36] $K_{\text{NN}} \simeq (J/\Delta^2)\nu_{nm}\nu_{n'm'}$. Compared with the usual flip-flop interaction strength between two qubits off-resonantly coupled to the same resonator mode, this coupling is a factor $J/|\Delta|$ smaller as it involves an additional off-resonant interresonator photon hopping. The interaction (7) acting for a duration T, naturally gives rise to the $\sqrt{i\text{SWAP}}$ gate when $K_{\text{NN}}T = \pi/4$. Two such gates together with single-qubit rotations can be used to implement the CNOT gates required for syndrome measurements in the surface code. As with the single-qubit gates, it is possible to perform many two-qubit gates in parallel by taking advantage of the electric field tunability of the qubit frequency. This is achieved by separating the qubits on the lattice into two sets with frequencies $\omega_Z^{(\text{r})}$ and $\omega_Z^{(\text{b})}$ as illustrated in Fig. 2. A full syndrome mapping cycle from the code qubits onto the ancilla qubits can then be performed in four steps.

Readout.—The readout of the ancilla qubits proceeds in standard fashion by homodyne detection of the dispersive phase shift incurred by reflected photons at the bare resonator frequency [19,42]. During readout the code qubits are decoupled from their resonators. Similar to single-qubit operations, readout of all ancilla qubits can be performed in parallel and does not require additional resonators, greatly simplifying the circuit design. The required reset of the ancilla qubits to their groundstate

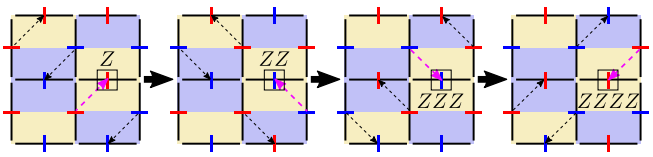

FIG. 2. Frequency layout for parallelization of syndrome mapping in four steps. Red (blue) bars denote qubits at frequency $\omega_Z^{(r)}$ ($\omega_Z^{(b)}$). The dashed black arrows indicate which couplings are resonant, i.e., active in a given configuration. The mapping of a $ZZZZ$ stabilizer is highlighted as an example (magenta arrows).

after measurement can be implemented for example by using the method of Geerlings *et al.* [43].

Parameter estimates.—For the simulations presented below we take $J = 159 \times 2\pi$ MHz, which corresponds to a coupling capacitance $C_c \simeq 14$ fF [36], and set the resonator frequency to $\omega_r = 13.35 \times 2\pi$ GHz. We further set $\omega_h = 28 \times 2\pi$ GHz, which for $m \simeq 0.012 m_e$, where m_e is the electron mass, corresponds to $x_{\mathrm{ZPF}} \simeq 166$ nm. We consider a magnetic field strength $B_\perp = 194$ mT and a zero-field g factor for Germanium [29,31] $g(E_z = 0) \simeq 5.5$. This yields a zero-field qubit frequency $\omega_Z(E_z = 0) \simeq 14.934 \times 2\pi$ GHz. The small length of the nanowires allows for a coplanar waveguide geometry with a small trench width, which we set to $W = 0.5$ μm. The vacuum field strength is consequently enhanced to $E_{\mathrm{rms}} \simeq 3.73$ V/m. Finally, we assume a Rashba spin-orbit parameter $\alpha_{\mathrm{DR}}/\hbar \simeq 10\ e(\mathrm{nm})^2 \times E_z$. For an applied field $E_z = 1$ V/μm, this corresponds to $\ell_{\mathrm{SO}} \simeq 635$ nm. According to Eq. (5), we thus estimate conservatively that coupling strengths between $\nu_{nm} = 0$ at $E_z = 0$ and $\nu_{nm} \simeq 40 \times 2\pi$ MHz at $E_z = 1$ V/μm are feasible. The corresponding qubit frequency shift between the "on" and the "off" states is $\Delta\omega_Z \simeq 1.161 \times 2\pi$ GHz, i.e., $\omega_Z(E_z = 1\ \mathrm{V}/\mu\mathrm{m}) \simeq 13.773 \times 2\pi$ GHz, which allows for phase gates on the nanosecond time scale.

Numerical simulations.—We characterize the theoretical performance of single and two-qubit gates on a 2×2 lattice in the presence of dissipation and gate imperfections by numerically solving the Lindblad master equation (with $\hbar = 1$)

$$\dot{\boldsymbol{\rho}} = -i[\boldsymbol{H} + \boldsymbol{H}_d, \boldsymbol{\rho}] + \kappa \sum_{nm} \mathcal{D}[\boldsymbol{a}_{nm}]\boldsymbol{\rho} + \gamma \sum_{nm} \mathcal{D}[\boldsymbol{\sigma}^-_{nm}]\boldsymbol{\rho}. \quad (9)$$

Here $\boldsymbol{H}$ is given by Eq. (6), κ denotes the single photon loss rate of the resonators, $\gamma = 1/T_1$ the qubit decay rate, and $\mathcal{D}[\boldsymbol{O}]\boldsymbol{\rho} = (2\boldsymbol{O}\boldsymbol{\rho}\boldsymbol{O}^\dagger - \boldsymbol{O}^\dagger\boldsymbol{O}\boldsymbol{\rho} - \boldsymbol{\rho}\boldsymbol{O}^\dagger\boldsymbol{O})/2$. Figure 3(c) shows the fidelity of a rotation the qubit at lattice site (0,0) around the x axis by angle π averaged over all initial states on the Bloch sphere as a function of the gate duration time T for $\kappa/h = \gamma/h = 10$ kHz. This rotation is realized by a drive on resonator (0,0) of the form $\boldsymbol{H}_d(t) = \varepsilon(t)(e^{i\omega_d t}\boldsymbol{a} + e^{-i\omega_d t}\boldsymbol{a}^\dagger)$ with frequency $\omega_d = \omega_Z + (2\bar{n}+1)\chi$ and Gaussian envelop $\varepsilon(t) = \varepsilon \exp[-(t-t_0)^2/(2\sigma^2)]$ with $\varepsilon = \pi\Delta/(2\sigma\nu\sqrt{2\pi})$. Here, $\sigma = T/5$, $t_0 = T/2$, $\Delta = \omega_Z - \omega_r$, and ω_Z is the bare qubit frequency in the "on" state with dispersive shift $\chi = \nu^2/\Delta$. The drive frequency shift $(2\bar{n}+1)\chi$ with $\bar{n} \simeq \varepsilon^2/[\Delta^2 + (\kappa/2)^2]$ corrects (approximately) for both the Lamb and Stark shifts. The simulated fidelity [full red curve in Fig. 3(c)] is upper bounded by $\mathcal{F}_\varphi = [1 + (1/3)e^{-\gamma T} + (2/3)e^{-[\gamma/2+\gamma_\varphi]T}]/2$ [dashed curve in Fig. 3(c)], which gives the average fidelity for an ideal gate with a T_1-limited qubit subject to photon shot noise induced dephasing [21] with rate $\gamma_\varphi \simeq 2\bar{n}\kappa(\pi/2)^2$ [blue curve in Fig. 3(c)]. The difference between the two curves is a measure of gate imperfections such as deviations from optimal pulse duration and spurious entanglement between the photons and the qubit, which increases with the drive strength.

Next we characterize the natural two-qubit gate generated by the interaction in Eq. (7). Figure 3(d) shows the fidelity of a $\sqrt{i\mathrm{SWAP}}$ gate between qubits at sites (0,0) and (0,1) obtained for $K_{\mathrm{NN}}T = \pi/4$, averaged over the subset

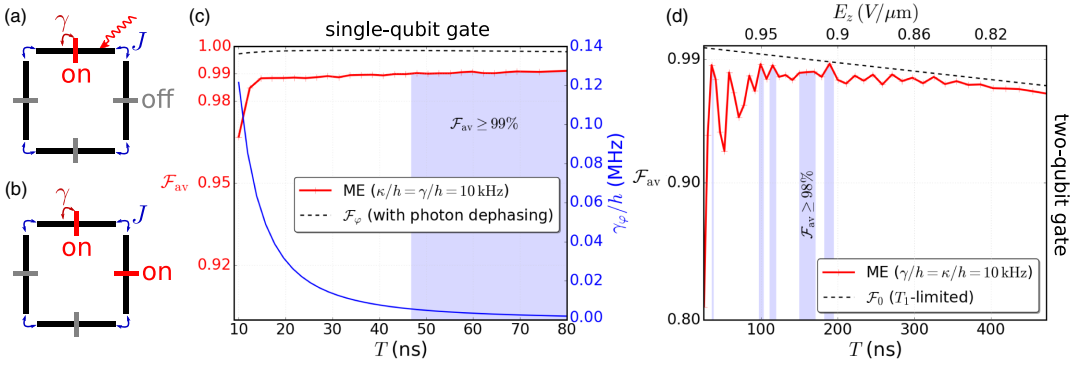

FIG. 3. Gate fidelity averaged over initial states on the Bloch sphere: $\mathcal{F}_{\mathrm{av}} = (1/4\pi)\int_0^{2\pi} d\varphi \int_0^{\pi} d\theta \sin(\theta)\mathcal{F}(\theta,\varphi)$, with $\mathcal{F}(\theta,\varphi) = \langle\theta,\varphi|\boldsymbol{\rho}(T)|\theta,\varphi\rangle$ and $|\theta,\varphi\rangle = \cos(\theta/2)|0\rangle + e^{i\varphi}\sin(\theta/2)|1\rangle$. (a) and (c) Single-qubit rotation around the x axis by angle π. Here $|0\rangle = |g\rangle_{00}$, $|1\rangle = |e\rangle_{00}$, the remaining qubits are initialized in their ground state. Only the qubit at (0,0) is coupled to its resonator with $E_z = 0.8$ V/μm and the drive strength is varied. The ideal gate unitary is $R_x(\pi) = e^{-i(\pi/2)\sigma^x_{00}}$. (b) and (d) Two-qubit $\sqrt{i\mathrm{SWAP}}$ gate. Here $|0\rangle = |g\rangle_{00}|e\rangle_{01}$, $|1\rangle = |e\rangle_{00}|g\rangle_{01}$, the other qubits are initialized in their ground state. The qubits at (0,0) and (0,1) are coupled to their resonators with varying but equal field strength E_z. The ideal gate unitary is $\sqrt{i\mathrm{SWAP}} = e^{-i(\pi/4)(\sigma^+_{00}\sigma^-_{01} + \sigma^-_{00}\sigma^+_{01})}$. Full curves are numerical results obtained by solving the master equation (ME) (9), and the dashed curves show analytic upper bounds for ideal gates [36].

of initial two-qubit states in span$\{|eg\rangle, |ge\rangle\}$, while the remaining two qubits are in their ground state. In this case, the gate duration T is fixed by the interaction strength. The latter, however, depends on the strength of the applied electric field E_z. For small E_z the averaged gate fidelity agrees well with that of an ideal T_1-limited $\sqrt{i\mathrm{SWAP}}$ gate, which for the considered initial states in the one-excitation manifold, is simply $\mathcal{F}_0 = e^{-\gamma T}$ [dashed curve in Fig. 3(d)]. As the field and hence the interaction strength is increased, the gate becomes faster and, at first, the fidelity increases. Because an increasing electric field also reduces the detuning between the qubit and the resonator, the dispersive approximation breaks down for too large an applied field, which is reflected in fluctuations and overall suppression of the fidelity at strong fields.

Conclusion.—We have proposed a scalable hybrid architecture for fault tolerant quantum computation via the surface code. The core of this system consists of a square lattice of capacitively coupled superconducting resonators, which serves as a two-dimensional quantum bus to mediate interactions between hole-spin qubits.

This work was supported by the Swiss National Science Foundation (SNSF) and the NCCR QSIT. We acknowledge discussions with Jelena Klinovaja, Christoph Kloeffel and James Wootton. The numerical computations were performed in a parallel computing environment at sciCORE scientific computing core facility at University of Basel using the Python library QuTip.

*Corresponding author.
simon.nigg@unibas.ch

[1] J. M. Taylor, H.-A. Engel, W. Dur, A. Yacoby, C. M. Marcus, P. Zoller, and M. D. Lukin, Nat. Phys. **1**, 177 (2005).
[2] Y. Chen *et al.*, Phys. Rev. Lett. **113**, 220502 (2014).
[3] K. Nemoto, M. Trupke, S. J. Devitt, A. M. Stephens, B. Scharfenberger, K. Buczak, T. Nöbauer, M. S. Everitt, J. Schmiedmayer, and W. J. Munro, Phys. Rev. X **4**, 031022 (2014).
[4] C. D. Hill, E. Peretz, S. J. Hile, M. G. House, M. Fuechsle, S. Rogge, M. Y. Simmons, and L. C. L. Hollenberg, Sci. Adv. **1**, e1500707 (2015).
[5] P.-M. Billangeon, J. S. Tsai, and Y. Nakamura, Phys. Rev. B **92**, 020509 (2015).
[6] T. Brecht, W. Pfaff, C. Wang, Y. Chu, L. Frunzio, M. H. Devoret, and R. J. Schoelkopf, npj Quantum Inf. Process. **2**, 16002 (2016).
[7] T. Karzig, C. Knapp, R. Lutchyn, P. Bonderson, M. Hastings, C. Nayak, J. Alicea, K. Flensberg, S. Plugge, Y. Oreg, C. Marcus, and M. H. Freedman, arXiv:1610.05289.
[8] L. A. Landau, S. Plugge, E. Sela, A. Altland, S. M. Albrecht, and R. Egger, Phys. Rev. Lett. **116**, 050501 (2016).
[9] S. Plugge, L. A. Landau, E. Sela, A. Altland, K. Flensberg, and R. Egger, Phys. Rev. B **94**, 174514 (2016).
[10] S. Bravyi and A. Kitaev, arXiv:quant-ph/9811052.
[11] F. Helmer, M. Mariantoni, A. G. Fowler, J. von Delft, E. Solano, and F. Marquardt, Europhys. Lett. **85**, 50007 (2009).
[12] D. P. DiVincenzo, Phys. Scr. **T137**, 014020 (2009).
[13] A. G. Fowler, M. Mariantoni, J. M. Martinis, and A. N. Cleland, Phys. Rev. A **86**, 032324 (2012).
[14] R. Barends *et al.*, Nature (London) **508**, 500 (2014).
[15] A. D. Corcoles, E. Magesan, S. J. Srinivasan, A. W. Cross, M. Steffen, J. M. Gambetta, and J. M. Chow, Nat. Commun. **6**, 6979 (2015).
[16] J. Kelly, R. Barends *et al.*, Nature (London) **519**, 66 (2015).
[17] M. Takita, A. D. Córcoles, E. Magesan, B. Abdo, M. Brink, A. Cross, J. M. Chow, and J. M. Gambetta, Phys. Rev. Lett. **117**, 210505 (2016).
[18] A. Blais, R.-S. Huang, A. Wallraff, S. M. Girvin, and R. J. Schoelkopf, Phys. Rev. A **69**, 062320 (2004).
[19] A. Blais, J. Gambetta, A. Wallraff, D. I. Schuster, S. M. Girvin, M. H. Devoret, and R. J. Schoelkopf, Phys. Rev. A **75**, 032329 (2007).
[20] J. Majer, J. M. Chow, J. M. Gambetta, J. Koch, B. R. Johnson, J. A. Schreier, L. Frunzio1, D. I. Schuster, A. A. Houck, A. Wallraff, A. Blais, M. H. Devoret, S. M. Girvin, and R. J. Schoelkopf1, Nature (London) **449**, 443 (2007).
[21] J. Gambetta, A. Blais, D. I. Schuster, A. Wallraff, L. Frunzio, J. Majer, M. H. Devoret, S. M. Girvin, and R. J. Schoelkopf, Phys. Rev. A **74**, 042318 (2006).
[22] J. Z. Blumoff, K. Chou, C. Shen, M. Reagor, C. Axline, R. T. Brierley, M. P. Silveri, C. Wang, B. Vlastakis, S. E. Nigg, L. Frunzio, M. H. Devoret, L. Jiang, S. M. Girvin, and R. J. Schoelkopf, Phys. Rev. X **6**, 031041 (2016).
[23] J. M. Gambetta, A. A. Houck, and A. Blais, Phys. Rev. Lett. **106**, 030502 (2011).
[24] S. J. Srinivasan, A. J. Hoffman, J. M. Gambetta, and A. A. Houck, Phys. Rev. Lett. **106**, 083601 (2011).
[25] C. Eichler, J. Mlynek, J. Butscher, P. Kurpiers, K. Hammerer, T. J. Osborne, and A. Wallraff, Phys. Rev. X **5**, 041044 (2015).
[26] G. Zhang, Y. Liu, J. J. Raftery, and A. A. Houck, arXiv:1603.01224.
[27] C. Kloeffel, M. Trif, and D. Loss, Phys. Rev. B **84**, 195314 (2011).
[28] Y. Hu, F. Kuemmeth, C. M. Lieber, and C. M. Marcus, Nat. Nanotechnol. **7**, 47 (2012).
[29] C. Kloeffel, M. Trif, P. Stano, and D. Loss, Phys. Rev. B **88**, 241405 (2013).
[30] J. H. Prechtel, A. V. Kuhlmann, J. Houel, A. Ludwig, S. R. Valentin, A. D. Wieck, and R. J. Warburton, Nat. Mater. **15**, 981 (2016).
[31] H. Watzinger, C. Kloeffel, L. Vukusic, M. D. Rossell, V. Sessi, J. Kukucka, R. Kirchschlager, E. Lausecker, A. Truhlar, M. Glaser, A. Rastelli, A. Fuhrer, D. Loss, and G. Katsaros, Nano Lett. **16**, 6879 (2016).
[32] R. Maurand, X. Jehl, D. K. Patil, A. Corna, H. Bohuslavskyi, R. Laviville, L. Hutin, S. Barraud, M. Vinet, M. Sanquer, and S. D. Franceschi, Nat. Commun. **7**, 13575 (2016).

[33] F. Maier, J. Klinovaja, and D. Loss, Phys. Rev. B **90**, 195421 (2014).
[34] C. Flindt, A. S. Sørensen, and K. Flensberg, Phys. Rev. Lett. **97**, 240501 (2006).
[35] M. Trif, V. N. Golovach, and D. Loss, Phys. Rev. B **75**, 085307 (2007).
[36] See Supplemental Material at http://link.aps.org/supplemental/10.1103/PhysRevLett.118.147701, which includes Ref. [37], for a derivation of Eqs. (3) and (4), electrostatic simulations of the lattice cross-capacitors, a derivation of the interresonator coupling term, a discussion of code folding and additional simulation results on single and two-qubit gate fidelities.
[37] M. A. Nielsen and I. L. Chuang, *Quantum Computation and Quantum Information* (Cambridge University Press, Cambridge, England, 2000).
[38] N. Samkharadze, A. Bruno, P. Scarlino, G. Zheng, D. P. DiVincenzo, L. DiCarlo, and L. M. K. Vandersypen, Phys. Rev. Applied **5**, 044004 (2016).
[39] F. Maier, C. Kloeffel, and D. Loss, Phys. Rev. B **87**, 161305 (2013).
[40] M. Brauns, J. Ridderbos, A. Li, E. P. A. M. Bakkers, and F. A. Zwanenburg, Phys. Rev. B **93**, 121408 (2016).
[41] G. Zhu, S. Schmidt, and J. Koch, New J. Phys. **15**, 115002 (2013).
[42] J. Koch, T. M. Yu, J. Gambetta, A. A. Houck, D. I. Schuster, J. Majer, A. Blais, M. H. Devoret, S. M. Girvin, and R. J. Schoelkopf, Phys. Rev. A **76**, 042319 (2007).
[43] K. Geerlings, Z. Leghtas, I. M. Pop, S. Shankar, L. Frunzio, R. J. Schoelkopf, M. Mirrahimi, and M. H. Devoret, Phys. Rev. Lett. **110**, 120501 (2013).